Supporting Information Appendix for: "Direct imaging of topological edge states in cold-atom systems"

N. Goldman,[1] J. Dalibard,[2,3] A. Dauphin,[1,4] F. Gerbier,[2] M. Lewenstein,[5,6] P. Zoller,[7,8] and I. B. Spielman[9]

[1] *Center for Nonlinear Phenomena and Complex Systems - Université Libre de Bruxelles (U.L.B.), B-1050 Brussels, Belgium*
[2] *Laboratoire Kastler Brossel, CNRS, ENS, UPMC, 24 rue Lhomond, 75005 Paris*
[3] *Collège de France, 11, place Marcelin Berthelot, 75005 Paris, France*
[4] *Departamento de Física Teórica I, Universidad Complutense, 28040 Madrid, Spain*
[5] *ICFO – Institut de Ciències Fotòniques, Parc Mediterrani de la Tecnologia, 08860 Barcelona, Spain*
[6] *ICREA – Institució Catalana de Recerca i Estudis Avançats, 08010 Barcelona, Spain*
[7] *Institute for Quantum Optics and Quantum Information of the Austrian Academy of Sciences, A-6020 Innsbruck, Austria*
[8] *Institute for Theoretical Physics, Innsbruck University, A-6020 Innsbruck, Austria*
[9] *Joint Quantum Institute, National Institute of Standards and Technology, and University of Maryland, Gaithersburg, Maryland, 20899, USA*

Appendix A: Time evolution and states population

In this study, the time evolution is chosen to be entirely dictated by the Hamiltonian $\hat{H}$, and thus, it is non-dissipative: after releasing the walls, the total energy of the system is constant and is given by

$$\mathcal{E}_0 = \langle\Psi_0|\hat{H}|\Psi_0\rangle \approx \sum_{E_\alpha<E_\mathrm{F}} E_\alpha, \tag{A1}$$

where we considered the approximation $\langle\Psi_0|\hat{H}|\Psi_0\rangle \approx \langle\Psi_0|\hat{H}_0|\Psi_0\rangle$, which is valid for V_hole sufficiently abrupt. For example, in the situation illustrated in Fig. 4, the energy released after removing the walls is about $J/3$. Therefore, in our calculations, the many-body state $|\Psi(t)\rangle$ never reaches the ground state $|\Psi_\mathrm{GS}\rangle$ of the final Hamiltonian $\hat{H}$, with energy

$$\mathcal{E}_\mathrm{GS} = \langle\Psi_\mathrm{GS}|\hat{H}|\Psi_\mathrm{GS}\rangle. \tag{A2}$$

This final ground state, which differs from the initially prepared ground state $|\Psi_0\rangle$ in Eq. (4), is expressed as

$$|\Psi_\mathrm{GS}\rangle = \prod_{\lambda=1}^{N_\mathrm{part}} \hat{a}_\lambda^\dagger|\emptyset\rangle, \tag{A3}$$

where $\hat{a}_\lambda^\dagger$ creates a particle in the single-particle state $|\phi_\lambda\rangle$, with energy $\epsilon_\lambda < \epsilon_{\lambda+1}$. Here, $N_\mathrm{part} = \sum_{E_\alpha<E_\mathrm{F}}$ is the total number of particles in the system, which is supposed to be constant (see Figs. A**a-b**). In our non-dissipative framework, the probability $\mathcal{P}_\lambda(t)$ of finding a particle in the eigenstate $|\phi_\lambda\rangle$ is constant and inferior to one, as it is simply given by

$$\mathcal{P}_\lambda(t) = \langle\Psi(t)|\hat{a}_\lambda^\dagger\hat{a}_\lambda|\Psi(t)\rangle = \sum_{E_\alpha<E_\mathrm{F}} |\langle\phi_\lambda|\chi_\alpha\rangle|^2 = \mathrm{cst} < 1,$$
$$\neq \langle\Psi_\mathrm{GS}|\hat{a}_\lambda^\dagger\hat{a}_\lambda|\Psi_\mathrm{GS}\rangle = 1 \text{ if } \lambda \leq N_\mathrm{part} \text{ (otherwise 0).} \tag{A4}$$

The populations $\mathcal{P}_\lambda$ are illustrated as a histogram in Fig. A**c**, for the case $\Phi = 1/5$ and $E_\mathrm{F} = -1.5J$. We find that when the Fermi energy is initially set within the first bulk gap, the population of high-energy dispersive bulk bands is highly limited during the evolution, which guarantees a clear spatial separation of the bulk and edge signal in this "topological quasi-flat band" configuration. The efficiency with which the initial edge modes χ_e project to the final edge modes ϕ_e is further shown in Fig. B, indicating the success of our scheme. For the situation illustrated in Figs. A-B, we find that the number of populated edge states $\mathcal{P}_\mathrm{edge} = \sum_{\lambda\in\text{edge states}} \mathcal{P}_\lambda \approx 30 \approx N_\mathrm{edge}/2$, where $N_\mathrm{edge} \approx 64$ is the number of populated edge states before removing the walls (see main text). This result is in agreement with the fact that the edge delimited by the bat contains $n^0_\mathrm{edge} \approx 2\times n_\mathrm{edge}$ sites, where $n_\mathrm{edge} \approx 2\pi r_0/a$ is the number of sites delimited by the external circular confinement.

In the main text, we discuss the non-dissipative evolution of the atomic cloud after releasing the walls V_hole, neglecting thermalization processes. However, it is instructive to estimate the energy loss that would be required to reach the ground state $|\Psi_\mathrm{GS}\rangle$, namely $\delta\mathcal{E} = \mathcal{E}_0 - \mathcal{E}_\mathrm{GS}$. We propose to evaluate this energy difference for a configuration which is particularly relevant for our work (see main text), namely, a system exhibiting large initial holes and a flat (dispersionless) lowest bulk band. In the following, we set the energy of the lowest bulk band equal to zero. The energy difference $\delta\mathcal{E}$ will generally be large in this "large hole/flat band" situation, since many bulk states become available in the lowest energy band after removing the walls, namely $\mathcal{E}_\mathrm{GS} \sim 0$ [see Figs. A**a-b** and below]. For this configuration, which is particularly suitable for visualizing the edge states encircling the holes, the energy difference is thus approximatively given by

$$\delta\mathcal{E} \approx \sum_{\text{occupied edge states } e} E_e, \tag{A5}$$

where we considered the Fermi energy to be located inside the first bulk gap [see Fig. A**a-b**]. For large holes $\eta = n_\mathrm{hole}/n_\mathrm{sites} \gg 0$, the final filling factor $\nu \ll 1/q$ such that the lowest bulk band will only be partially occupied when reaching the ground state $|\Psi_\mathrm{GS}\rangle$, and thus $\mathcal{E}_\mathrm{GS} \sim 0$. From a rough geometric argument, we expect about $N_\mathrm{edge} \sim \pi R_F(2+\sqrt{\eta})/a(q-1)$ available edge states in

the lowest bulk gap of the initial system. Approximating the edge-state branch as being linear inside the whole gap Δ, we find

$$\delta\mathcal{E} \sim \frac{\Delta\pi}{q-1}(R_F/a)(1+0.5\sqrt{\eta}), \tag{A6}$$

which corresponds to an energy difference $\delta\mathcal{E} \sim 1.5(R_F/a)J$ in the case $\Phi = 1/5$ and $\eta = 1/\sqrt{2}$ (see main text). In a typical experiment, $R_F \sim 100a$, which would require an important energy loss $\delta\mathcal{E} \sim 150J$ to reach the ground state $|\Psi_{\rm GS}\rangle$. We verified that the estimated energy difference $\delta\mathcal{E}$ in Eq. (A6) is in good agreement with a direct numerical evaluation of Eq. (A5), for the system illustrated in Fig. 4 (i.e., $\Phi = 1/5$, $\eta \approx 1/\sqrt{2}$ and $E_{\rm F} = -1.5J$). As illustrated in Fig. A**b**, the ground state $|\Psi_{\rm GS}\rangle$ generally consists in a partially occupied bulk band, which indicates that the edge states will no longer be populated if the system relaxes to the ground state $|\Psi_{\rm GS}\rangle$. Therefore, our scheme requires that the system remains in an excited state during the time evolution, namely, that dissipation should be limited.

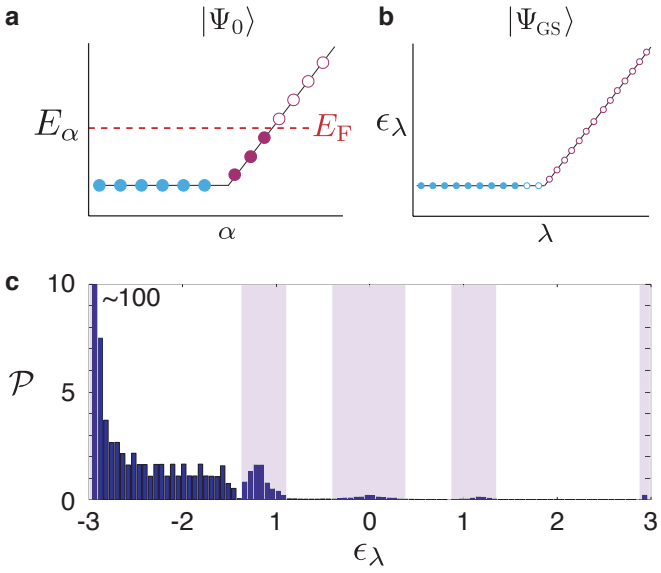

FIG. A: **Ground states and single-particle states population.** Comparing **a,** the groundstate $|\Psi_0\rangle$ of the initially prepared system (with holes) and **b,** the groundstate $|\Psi_{\rm GS}\rangle$ of the final system (without holes). Filled and empty blue (red) dots represent the occupied and unoccupied bulk (edge) states, respectively, with occupation number = 1. Note that the total number of particles, $N_{\rm part} = \sum_{E_\alpha<E_{\rm F}}$, is constant. **c** The population $\mathcal{P}$ of the states $|\phi_\lambda\rangle$, as a function of their energy ϵ_λ, as established by the Fermi energy $E_{\rm F} = -1.5J$ for the case illustrated in Fig. 4 (i.e., $\Phi = 1/5$, $\gamma = \infty$, $r_0 = 27a$ and $\eta \approx 0.7$). The energies corresponding to bulk states are emphasized by purple shaded regions, see Fig. 2**b**.

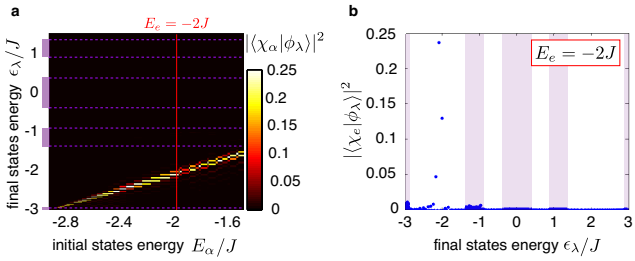

FIG. B: **Wave-function overlaps between initial and final states. a,** The overlap $|\langle\chi_\alpha|\phi_\lambda\rangle|^2$ between the eigenstates of the initial (χ_α) and final (ϕ_λ) Hamiltonians, represented as a function of their energies. The parameters are the same as in Fig. A. Note that the edge states are found in the bulk gap, namely, within the range $E \approx [-2.9J, -1.3J]$. **b,** Cut through the plot in Fig. **a**, for a specific initial edge state with energy $E_e = -2J$. The initial edge modes effectively project to the final edge modes, highly limiting the population of high energy (dispersive) bulk states. The energies corresponding to bulk states are emphasized by purple shaded regions in **a** and **b**.

Appendix B: The opposite-flux method for dispersive bulk bands

In this Section, we discuss how the difference $\delta\rho(\boldsymbol{x},t) = \rho(\boldsymbol{x},t;+\Phi) - \rho(\boldsymbol{x},t;-\Phi)$, obtained from two successive measurements with opposite magnetic fluxes, is related to the edge states contributions $\rho_{\rm edge}(\boldsymbol{x},t;\pm\Phi)$. We show in Fig. C**a**, the evolution of $\delta\rho(\boldsymbol{x},t)$ for the dispersive case $\Phi = 1/3$, which clearly indicates that the contributions from the bulk $\rho_{\rm bulk}(\boldsymbol{x},t;+\Phi) \approx \rho_{\rm bulk}(\boldsymbol{x},t;-\Phi)$ vanish from the signal at all times $t = 7 - 70\hbar/J$. Accordingly, $\delta\rho(\boldsymbol{x},t) \approx \rho_{\rm edge}(\boldsymbol{x},t;+\Phi) - \rho_{\rm edge}(\boldsymbol{x},t;-\Phi)$. To clarify the evolution of this signal, which has non-vanishing values in the vicinity of the Fermi radius R_F, we show the chiral evolution of the edge states contribution $\rho_{\rm edge}(\boldsymbol{x},t;\pm\Phi)$ in Figs. C**b-c**. At small times, the overlap between the two contributions $\rho_{\rm edge}(\boldsymbol{x},t;\pm\Phi)$ decreases in time, leading to a progressive broadening of the signal $\delta\rho(\boldsymbol{x},t)$ along the 1D circular edge. Then, after reaching a rotation of $\theta \approx \pi/4$, the overlap increases, and eventually leads to a vanishing of the signal $\delta\rho(\boldsymbol{x},t) \approx 0$ when the edge states have undergone a rotation of $\pi/2$, where $\rho_{\rm edge}(\boldsymbol{x},t;+\Phi) \approx \rho_{\rm edge}(\boldsymbol{x},t;-\Phi)$. In Fig. C, this happens at time $t^* \approx 49\hbar/J$, indicating that the edge states angular velocity is $\dot{\theta} \approx 0.03J/\hbar$ for $R_F = 27a$. The opposite-flux method therefore offers a general technique for emphasizing the existence of chiral edge states in dispersive systems, and also, for evaluating their characteristic angular velocity.

We verified that a slight difference in the filling, $E_{\rm F}(\Phi_+ = +1/3) \approx E_{\rm F}(\Phi_- = -1/3) \pm 0.1J$, or variations in the flux, $\Phi_+ = 1/3$ and $\Phi_- \approx -\Phi_+ \pm 0.01$, does not significantly affect the signal $\delta\rho(\boldsymbol{x},t)$ shown in Fig. C **a**, highlighting the robustness of this method against possible experimental imperfections.

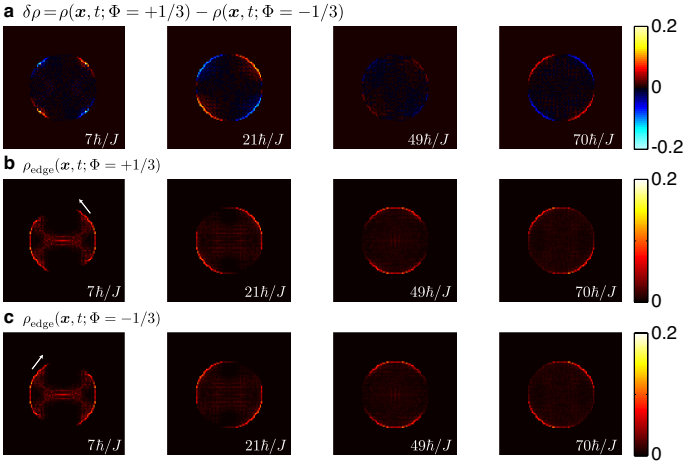

FIG. C: **The opposite-flux method for dispersive systems. a,** Evolution of the difference $\delta\rho = \rho(\boldsymbol{x},t;\Phi = +1/3) - \rho(\boldsymbol{x},t;\Phi = -1/3)$, for the same configuration as in Figure 3. **b,** Evolution of the initially populated edge states $\rho_{\rm edge}(\boldsymbol{x},t)$ for $\Phi = +1/3$, and **c,** for $\Phi = -1/3$. The vanishing of the signal $\delta\rho(\boldsymbol{x}) \approx 0$ corresponds to a rotation of $\pi/2$. This happens at time $t^* \approx 49\hbar/J$, indicating that the edge state angular velocity is $\dot{\theta} \sim 0.03J/\hbar$ for $R_F = 27a$.

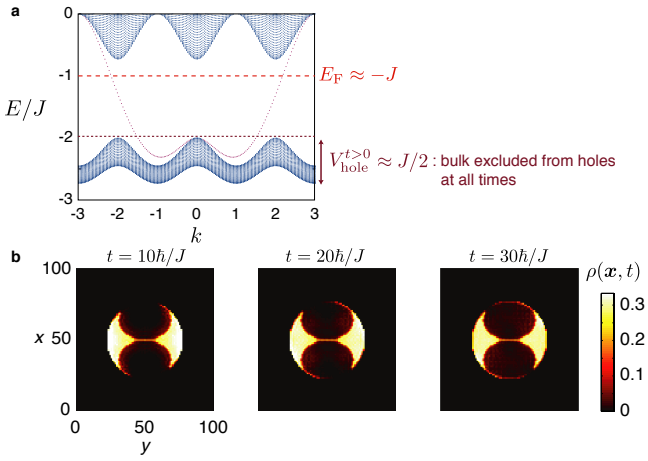

FIG. D: **The edge-filter method for dispersive systems. a,** Energy spectrum $E(k)$ as a function of the quasi-momentum k for $\Phi = 1/3$. Also shown are the typical Fermi energy and the final walls potential strength $V_{\rm hole}^{t>0} \approx W$, where W is the width of the lowest bulk band. **b,** Evolution of the spatial density $\rho(\boldsymbol{x},t)$ for $\Phi = 1/3$, $E_{\rm F} = -0.85J$, and infinitely abrupt confinement/walls. At $t = 0$, the strength of the walls potential is suddenly reduced to $V_{\rm hole}^{t>0} = 0.5J$. Note that most of the bulk states are excluded from the holes during the evolution, yielding a clear edge-state signal, to be compared with Fig. 3 **a**.

Appendix C: The edge-filter method for dispersive bulk bands

Another strategy consists in allowing the edge states to propagate at $t > 0$, while *forbidding* the bulk states to penetrate the regions initially occupied by the holes. This can be achieved by suddenly lowering the additional potential walls $V_{\rm hole}$ to some intermediate value $V_{\rm hole}^{t>0} \neq 0$, instead of removing them completely at $t = 0$. This "edge-filter" scheme is illustrated in Fig. D**a**, for the dispersive case $\Phi = 1/3$. By suddenly lowering the walls potential to the value $V_{\rm hole}^{t>0} \approx W$, where W is the width of the lowest bulk band, we limit the undesired filling of the holes by the bulk states at times $t > 0$. In contrast, the populated edge states with energy $\epsilon_e > V_{\rm hole}^{t>0} + \epsilon_{\rm min}$, where $\epsilon_{\rm min}$ is the minimum of the bulk band, are allowed to propagate around the holes without being spoiled by the bulk. The resulting time evolution of the density $\rho(\boldsymbol{x},t)$, presented in Fig. D**b**, shows a clear propagation of the edge states around the holes. Experimentally, this method offers an efficient method to isolate the edge states contribution from the spoiling bulk background, but it necessitates a very precise control over the potential strength $V_{\rm hole}$.

Appendix D: Sensitivity to imperfect filling

Our general scheme is based on the possibility of preparing a QH atomic state, which can be achieved by generating a magnetic flux Φ in the lattice and filling the lowest bulk band completely. In other words, one has to tune the total number of particles $N_{\rm part}$ in such a way that the Fermi energy $E_{\rm F}$ lies within the lowest bulk gap. According to the topological nature of the lowest bulk band, one is then guaranteed that topological edge states are populated. In practice, the total number of particles (and the corresponding Fermi energy $E_{\rm F}$) can be tuned with a great precision in cold-atom experiments. However, it is instructive to test the robustness of our method against inexact filling effects, in particular, for the dispersionless case $\Phi = 1/5$. We remind that in this configuration, the clear separation of the bulk and edge states contributions to the density relies on the fact that the bulk states are dispersionless (they are described by a quasi-flat band). Here, we show that this picture holds even when the second (dispersive) bulk band is dramatically filled, see Fig. E. From this result, we find that the high-energy bulk states contribute in a non-chiral manner to the density evolution, see Fig. E, and that their dispersive motion is slow compared to the edge states propagation along the circular boundary. In particular, this shows that the chiral picture drawn by the density $\rho(\boldsymbol{x},t)$, and which will be imaged in an experiment, can unambiguously be attributed to the populated edge states. We conclude that the edge-state signal obtained for the interesting case $\Phi = 1/5$ remains clear and detectable, as long as sufficiently many edge states are initially populated. In particular, this indicates that our scheme is robust at finite temperature $T > 0$, as long as it remains small compared to the gap's width Δ, in order to insure a sufficiently large edge-state population.

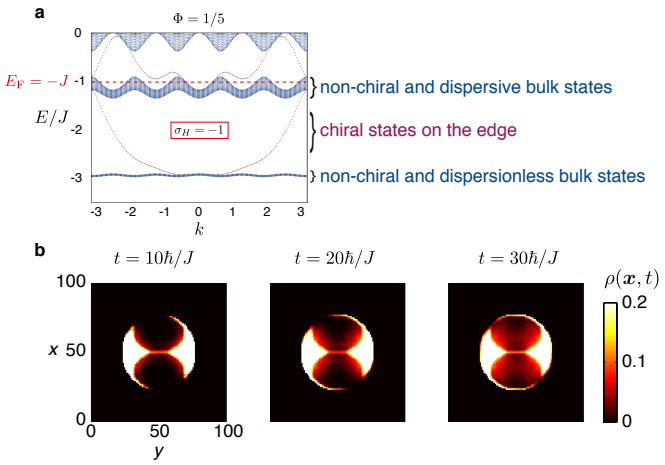

FIG. E: **Sensitivity to imperfect filling in the flat-band configuration. a,** Energy spectrum $E(k)$ as a function of the quasi-momentum k for $\Phi = 1/5$, indicating the "dramatic" Fermi level $E_F = -J$ used in **b**, as well as the characteristics of the occupied states. **b,** Evolution of the spatial density $\rho(\boldsymbol{x}, t)$ for $E_F = -J$ and infinitely abrupt confinement/walls. Note the non-chiral behavior of the dispersive bulk states, to be compared with Fig. 4 **a**.

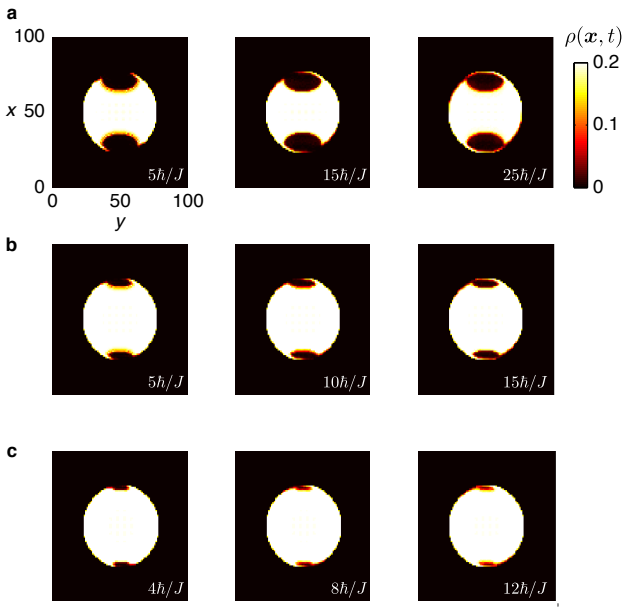

FIG. F: **Effects of the holes size.** The spatial density $\rho(\boldsymbol{x}, t)$ for $\Phi = 1/5$, $E_F = -1.5J$, $r_0 = 27a$ and $\gamma = \infty$. The holes are described by Eq. (E1) and correspond to **a,** $b = 4$, **b,** $b = 8$, and **c,** $b = 16$. Note that the chiral motion of the edge states is still visible, even in the limit of tiny perturbative walls V_{hole}.

Appendix E: The holes geometry and size effects

Our setup illustrated in Fig. 1 features two large repulsive potentials, which create the initial bat geometry. These holes are chosen to be created by infinitely abrupt walls V_{hole}, which are delimited by the two ellipses

$$(x \pm r_0/2)^2 + (y/\sqrt{2})^2 = r_0^2/4,$$

where the coordinates $(x, y) = 0$ at the center of the trap. This choice is motivated by the fact that these walls coincide (up to first order) with the external circular wall $V_{\text{conf}}(r)$ of radius r_0, in the vicinity of the poles located at $(\pm r_0)\mathbf{1}_{\boldsymbol{x}}$. Note that in the following of this discussion, we consider that $V_{\text{conf}}(r) \propto (r/r_0)^\gamma$ with $\gamma = \infty$.

The geometry produced by these potentials is particularly suitable to emphasize the edge states motion at time $t > 0$, as they encircle the regions initially surrounded by the elliptical walls. However, in this exotic geometry, the large holes correspond to a massive distortion of the standard circular system. It is thus interesting to study the validity of our method, as we progressively reduce the size of the holes. Here, we demonstrate that our scheme still shows a clear manifestation of the edge states, even in the limit where the walls V_{hole} only represent a small perturbation of the system, in the vicinity of its circular boundary. To analyze this, we propose to calculate the time evolution of the density $\rho(\boldsymbol{x}, t)$ after removing the elliptical walls delimited by the more general equations

$$\big(x \pm (b-1)\, r_0/b\big)^2 + \big(y/\sqrt{b}\big)^2 = (r_0/b)^2, \qquad \text{(E1)}$$

which can be made arbitrarily small ($b \gg 1$), while maintaining the smooth contact with $V_{\text{conf}}(r)$ at the poles. The results are shown in Fig. F for the flat-band configuration previously studied in Fig. 4 (for $b = 2$), but with smaller initial holes $b = 4, 8, 16$. This picture emphasizes the fact that our scheme still allows to detect the chiral motion of the edge states, in the limit of small perturbative walls V_{hole}. However, we stress that it is crucial to prohibit any broadening of the edge state signal in the perturbative regime $b \gg 2$, which necessarily requires the use of an extremely abrupt external potential V_{conf} with $\gamma \sim \infty$. Moreover, considering smaller holes also demands to further reduce the bulk dispersion, which can be achieved by considering the quasi-flat-band configuration $\Phi = 1/5$, see Fig. F, or by exploiting the "opposite-flux" or "edge-filter" methods.

Another relevant configuration is obtained by replacing the constraining potentials V_{hole} by a spacious wall V_{edge} that initially confines the entire atomic cloud to a small region located in the vicinity of the circular edge delimited by $V_{\text{conf}}(r)$, see Fig. G. After releasing the wall V_{edge} at time $t = 0$, the edge states propagate along the circular edge delimited by $V_{\text{conf}}(r)$, while the bulk states evolve towards the center of the trap. This strategy, which largely improves the edge/bulk ratio, is particularly efficient for dispersionless systems (e.g. $\Phi = 1/5$).

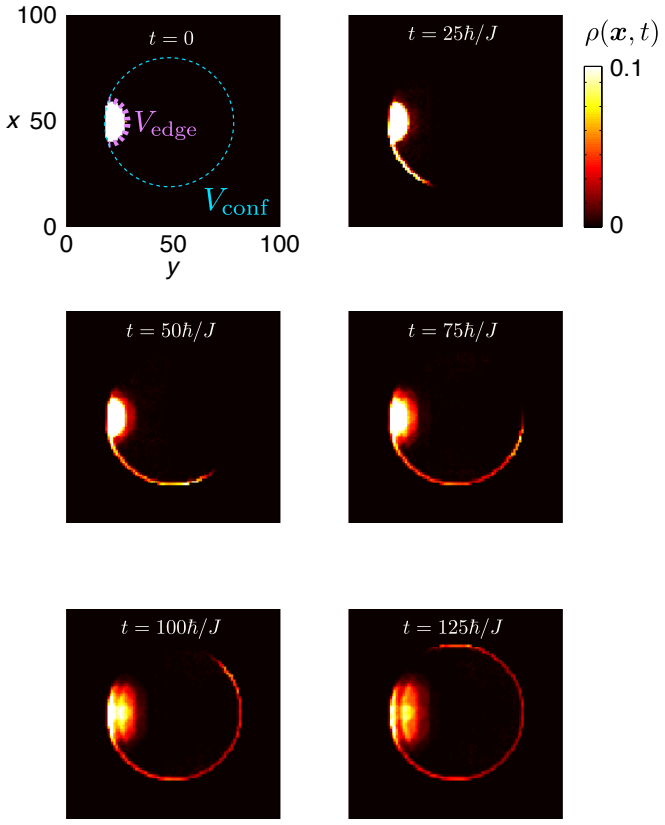

FIG. G: **Preparing the atomic cloud close to the edge.** The spatial density $\rho(\boldsymbol{x}, t)$ for $\Phi = 1/5$, $E_{\rm F} = -1.5J$, $r_0 = 32a$ and $\gamma = \infty$. The system is initially confined close to the circular edge at $r = r_0$ by an abrupt potential wall $V_{\rm edge}$. After releasing the wall $V_{\rm edge}$, the edge states propagate along the circular edge delimited by $V_{\rm conf}(r)$, highlighted in the top-left picture by a blue dotted circle.

Appendix F: Time evolution of a trivial insulating phase

The chiral motion of the edge states shown in Figs. 3 and 4 is a signature of the non-trivial Chern number $\nu = -1$ (see main text). As illustrated in Fig. 5, reversing the sign of the magnetic flux $\Phi \to -\Phi$ leads to an opposite chirality, in agreement with the fact that the Chern number also changes its sign under the transformation. Here, we further demonstrate that the edge-states motion, visible in the time-evolving density $\rho(\boldsymbol{x}, t)$, can be unambiguously attributed to the non-triviality of the Chern number. We consider the same system, but in a configuration characterized by a *trivial* Chern number $\nu = 0$. This configuration is produced in the following way: (i) We set the flux to the value $\Phi = 1/2$, which leads to a gapless bulk energy spectrum displaying two Dirac cones. (ii) We add a staggered potential along both spatial directions, with alternating on-site energies $\pm V_{\rm stag}$, which opens a bulk gap around $E = 0$. This gap is trivial in the sense that the lowest band is associated with a zero Chern number $\nu = 0$, and therefore, edge states are unexpected in this configuration. We represent in Fig. H the time-evolving density, obtained by initially setting the Fermi energy within the trivial gap. This figure H, which is to be compared with Fig. 3, shows (i) the *non-chiral* dynamics of the bulk states initially occupying the lowest band, and (ii) the absence of chiral edge states.

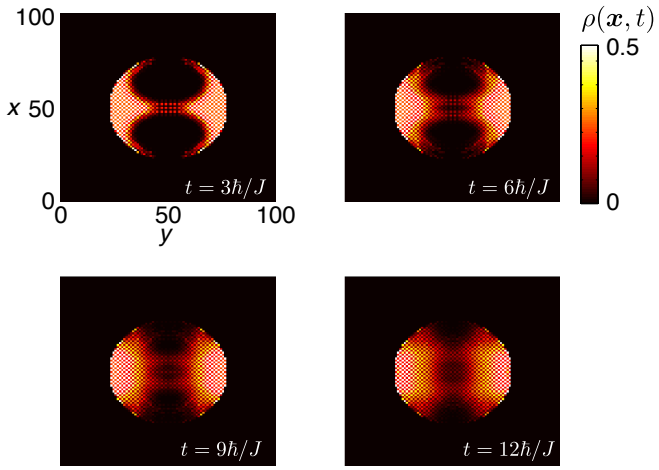

FIG. H: **Time evolution of a trivial insulating phase.** The spatial density $\rho(\boldsymbol{x}, t)$ for $\Phi = 1/2$, $r_0 = 27a$ and $\gamma = \infty$. The Fermi energy $E_{\rm F} = 0$ is set within a trivial bulk gap ($\nu = 0$), opened by a staggered potential of strength $V_{\rm stag} = J$. Chiral edge states are absent in the time-evolving density, in agreement with the triviality of the Chern number $\nu = 0$.